POLITECNICO DI TORINO
Repository ISTITUZIONALE

MODELING A SUBJECT WEARING AN INDUSTRIAL TRUNK SUPPORT EXOSKELETON

Original
MODELING A SUBJECT WEARING AN INDUSTRIAL TRUNK SUPPORT EXOSKELETON / Eula, G.. - In: INTERNATIONAL JOURNAL OF MECHANICS AND CONTROL. - ISSN 1590-8844. - 26:1(2025), pp. 103-118. [10.69076/jomac.2025.0010]

Availability:
This version is available at: 11583/3003132 since: 2025-09-18T11:17:48Z

Publisher:
ASTRA M B

Published
DOI:10.69076/jomac.2025.0010

Terms of use:

This article is made available under terms and conditions as specified in the corresponding bibliographic description in the repository

Publisher copyright

(Article begins on next page)

19 November 2026

ISSN 1590-8844
International Journal of Mechanics and Control, Vol. 26, No. 01, 2025
https://doi.org/10.69076/jomac.2025.0010

MODELING A SUBJECT WEARING AN INDUSTRIAL TRUNK SUPPORT EXOSKELETON

Gabriella Eula*

* Department of Mechanical and Aerospace Engineering, Politecnico di Torino, Torino Italy

ABSTRACT

The paper presents a model of a human body wearing an industrial trunk support exoskeleton based on a pneumatically actuated prototype designed and constructed at the Politecnico of Turin Department of Mechanical and Aerospace Engineering (DIMEAS). Developed using commercial software, this innovative model was used to investigate the movement, mass and inertia parameters of the wearer's trunk with and without the exoskeleton. These considerations are always very important for control system design. Actuation units are located at each hip joint, consist of pneumatic motors and toothed belt drives, and feature a particular structure to respect the physiological difference between the hip joint and the lumbo-sacral joint. Preliminary simulation results are in good agreement with the results obtained from earlier numerical models. The simulation technique illustrated here is faster than previous approaches, as a CAD human body model can be imported directly into a software environment and then evaluated.

Keywords: industrial trunk support exoskeleton; operator wearing a trunk exoskeleton model; industrial trunk support exoskeleton with pneumatic actuation; active industrial exoskeleton

1 INTRODUCTION

Industrial exoskeletons continue to make progress in a wide range of applications [1, 3].They can be designed for full-body use [4], for lower limbs only [5-8], or for the upper body, i.e., trunk or upper limbs [9-14]. Functions can include assisting the wearer while working in a seated position or bending forward, while handing or moving loads, while holding demanding postures with raised arms for prolonged periods, etc. The structure of industrial exoskeletons must be robust and lightweight to ensure strength as well as wearer comfort. In most cases this is achieved by using aluminum alloys or composite materials. The structure includes joints so that the device can move smoothly and naturally along with the wearer's body. The force needed to perform the tasks for which industrial exoskeletons are designed is provided by pneumatic, hydraulic or electric actuators.

Contact author: Gabriella Eula[1]

[1] Corso Duca Degli Abruzzi 24, Torino, TO, 100129, Italy
E-mail: gabriella.eula@polito.it

Actuators are controlled by an electronic system which is based on special algorithms and interprets the data provided by sensors. Such exoskeletons feature a single battery power source. A major benefit of these exoskeletons is that they reduce musculoskeletal loading and fatigue, thus lowering the risk of injury to the wearer [15]. In designing exoskeleton control systems, it is essential to consider all parameters, inertia properties in particular [16,17]. Accordingly, this study included an analysis of the inertial aspects, whose findings were in full agreement with others presented in the literature for the human body shape and position considered here. A number of dynamic considerations must be borne in mind in assessing the motor torque applied to the human body joints. Often these dynamic actions influence the required torque numerical value, so it is better to examine a static equilibrium condition [11-14] during the design process of the actuation units and their power. Exoskeletons are used for a wide range of purposes, including military [3], rehabilitation/assistance training [2, 5, 6] and industrial applications [9, 11-14]. In many industrial operations, robotic devices can help workers improve performance and prevent musculoskeletal strain and fatigue. Many of these exoskeletons provide the wearer with a percentage of the maximum required muscle torque. In addition to the ability to deliver this percentage of the required maximum torque,

these machines must accommodate working conditions calling for total maximum torque or legs-free operation. The latter operating mode allows the wearer's legs to move freely in the event of an emergency or during tasks calling for independent leg movement [11-14]. This paper presents a simulation model constructed in a commercial software environment. The model was used first to analyze the wearer's entire body, and then to analyze the body together with the DIMEAS (Department of Mechanical and Aerospace Engineering, Politecnico of Turin, Italy) trunk exoskeleton. The exoskeleton was designed to support the wearer's trunk in tasks requiring flexion, extension, or bending forward while stationary for prolonged periods.

This study was conducted to develop a reliable model for use in analyzing how the wearer and exoskeleton systems function together. It was based on previous work by the authors on several types of exoskeleton [2, 5-7, 11-14]. In view of the importance of inertia parameters [18-29] for exoskeleton operation, the authors used a software environment to construct a model of the entire human body and then of the human body wearing the DIMEAS industrial trunk support exoskeleton. These models can be used to assess inertial actions and their influence while varying the main parameters. Comparison with the data presented in the literature [16, 17-29] confirmed the models' reliability. The models' operation was evaluated through a comparison with previous experimental tests on trunk flexion and with earlier numerical models developed by the authors using other software. These comparisons all yielded satisfactory results, and suggested a strategy for future exoskeleton design.

2 BRIEF DESCRIPTION OF THE DIMEAS EXOSKELETON PROTOTYPE

The exoskeleton considered here is an active industrial trunk support exoskeleton designed and constructed at DIMEAS [12,13]. Figure 1a shows the prototype as worn. The exoskeleton consists of two pneumatic actuation units on the hip joint axis (A) which assist the wearer during trunk movement; a rigid backframe structure (B) carried on the wearer's back to provide support; and two leg-links (C) worn in contact with the thigh to support part of the load. Figure 1b is a photograph of the DIMEAS prototype. Actuation unit details are shown in Figure 1c, where (1) is the pulley connected to the pneumatic motor; (2) is the pulley connected to the backframe and representing the actuation unit joint for the physiological lumbosacral joint; (3) is the first toothed belt; (4) is the hip joint pulley connected to the leg-link; (5) is the second toothed belt; and (6) is a detail of the backframe bar. Using two toothed belt drives enables the exoskeleton structure to reproduce the physiological difference between the hip joint and the lumbosacral joint. This is important in order to ensure physiological trunk movement on the part of the wearer. Figure 1d shows the main elements of the exoskeleton and the human body parts involved.

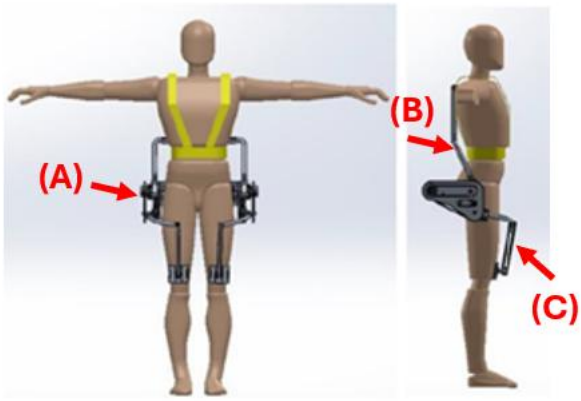


Figure 1a The exoskeleton prototype as worn.



Figure 1b The DIMEAS prototype.

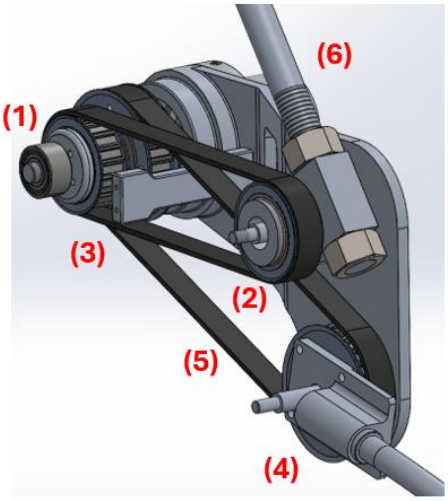


Figure 1c Hip actuation unit details.

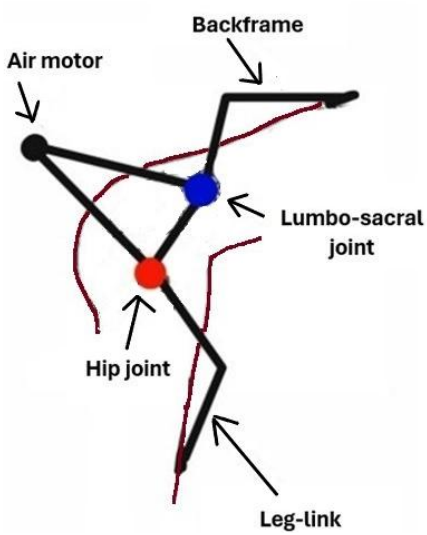


Figure 1d Schematic diagram of the main human and exoskeleton parts.

Pneumatic actuation was chosen for safety purposes. In addition, it makes it possible to control applied torque by varying air motor supply pressure, and to lock the exoskeleton in any trunk flexion position desired by the wearer by pressurizing both air motor chambers. The authors modeled the exoskeleton and the wearer's body in a commercial software environment (Simcenter Amesim [30]) which is often used to simulate mechanical systems. The actuation units were also analyzed.

3 THE MODELS

Using a specific software tool, the authors imported in Simcenter Amesim environment [30]: a model of the human body obtained from free web archives [31] (here called model A); a model of the human body constructed using a CAD software (SOLIDWORKS® 2023) and designed using physiological information from the literature [32] (here called model B). Figure 2 shows human body model A wearing the exoskeleton, as uploaded in Simcenter Amesim.

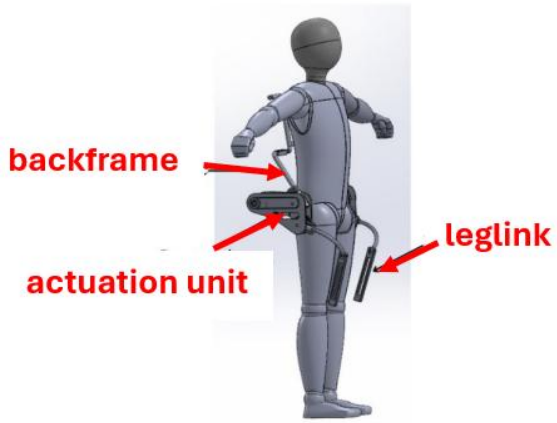


Figure 2 CAD human body model A wearing the exoskeleton.

These human bodies were analyzed alone and then wearing the exoskeleton. Choosing appropriate modeling parameters to ensure correct simulation was a key part of the study.

4 THE BODY MODEL

To simulate the "wearer + exoskeleton" system in the Simcenter Amesim environment, the human body model was first studied without the exoskeleton. This step was important in selecting the best simulation parameters, with particular attention to the inertial aspects. The properties shown in Table I were used to simulate body parts [32,33].

Table I - Density of the human parts considered here

Body part	Density (kg/m^3)
Forearm and hand	1140
Arm	1070
Foot and leg	1090
Thigh	1050
Head and neck	1110
Trunk	1030

Trunk mass was 59.43 kg. The other parameters used for the simulation are illustrated in the following paragraphs. Two models of the human body were developed and studied in the software environment, with particular attention to inertia properties. Both human body models represent a 95th percentile adult Italian male [32-35]. For all simulations in the Simcenter Amesim environment, both of the human body model's arms were in abduction. The human body model was separated into two subsystems, one for the upper body, and the other for the lower body. The sections were connected by means of the hip joint. Each subsystem has its own center of mass. The decision to model two subsections was motivated by the type of movement investigated, viz., trunk flexion followed by extension, with limited leg rotation. Accordingly, the movement of interest here is that of the trunk, not that of the entire body.

4.1 BODY MODEL A

Figure 3a shows CAD body model A [31]. In this figure and in the following description, the exoskeleton is not worn. This CAD model was imported in Simcenter Amesim. In particular, tools called "ports" were used. In Simcenter Amesim, ports are the points of connection between two subsystems using the same joint, which also enables them to move relative to each other. Figure 3b shows the ports set for the upper body: port A is the connection with the hip joint to move the trunk, and is also connected to port D on the legs; port B is the connection between the trunk and the backframe.

Figure 3c shows the ports set for the lower body: port D is the connection with the hip joint for trunk movement; ports B and C are the connections between the two leg-links and the exoskeleton; port A is the connection with the ankle joint.

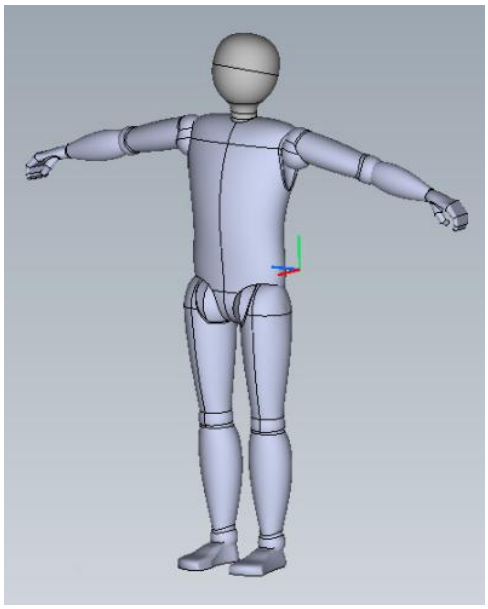


Figure 3a CAD human body model A.

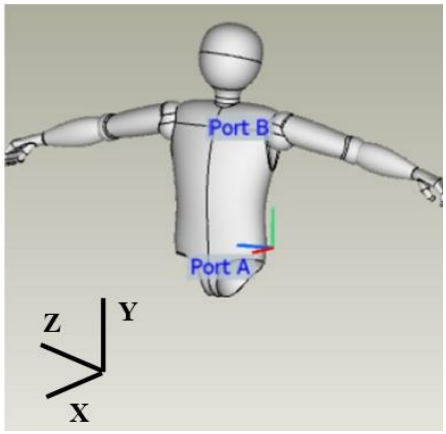


Figure 3b Upper body ports.

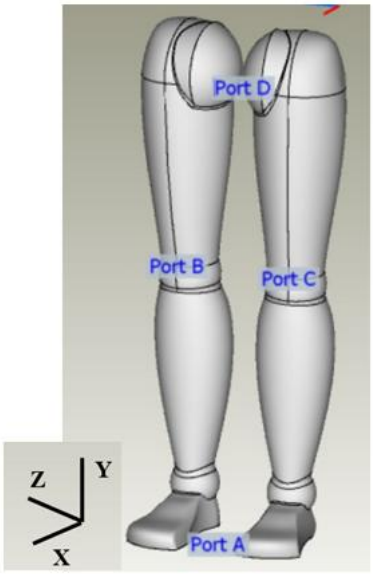


Figure 3c Lower body ports.

The upper and lower body were connected using a controlled hinge in each hip joint which receives an input torque that provides the control signal for the movement. A similar controlled hinge was also set between the legs and the ground in order to simulate leg movement relative to the trunk. The main purpose of this simulation is to assess total muscle torque on the hip joints. The assembly process is purely numerical and hidden from the user, but a sketch viewer in the icon can be used to see the result of this process, as shown in Figure 4. The two subsystems set in the software are as shown in Figure 4, where the two rigid bodies are connected by the hinge representing the hip joint and the second hinge is connected to the zero velocity source, i.e., to the ground. Each shape has its center of mass, yellow points in Figure 4.

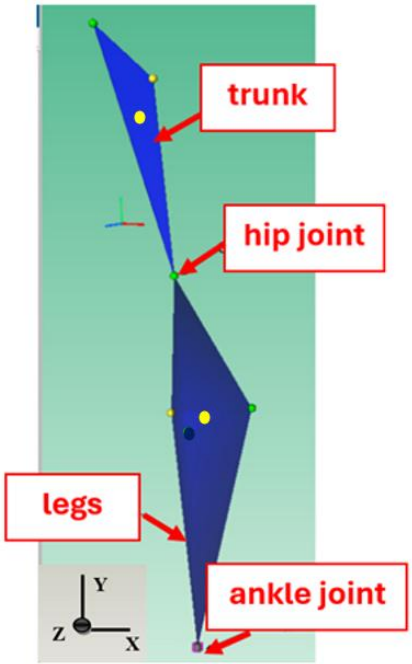


Figure 4 Visualization of the human body (model A) assembled in Simcenter Amesim.

The anomalous shape of the bodies is due to the fact that the assembly algorithm is based on the positions of the centers of mass (represented in Figure 4 as yellow points) and connection ports (represented here as green points). The legs protrude more at the height of the knee, as the body port coordinates were modified to make them coincide with those of the end of the leg-link. This was necessary because at this stage the CAD model does not include the leg strap that secures the leg-link to the wearer's legs, so the strap could not be imported to Simcenter Amesim. This does not affect the simulation, as the mass and the inertia matrix are still those of the CAD model, but it is important to simulate the effective contact between the two bodies. In the simulation with the body model alone, the only connection ports that can be used to simulate movement are those for the legs, those connected to the ground thanks to the zero velocity source (bottom of Figure 4) and those connecting with the torso through the hip joint

(bottom of Figure 4). For the trunk, the only port used is that which connects it to the legs through the hip joint. The uppermost port (green dot at the top in Figure 4) was used for connection to the exoskeleton backframe. In practice, the connection ports serve to obtain the geometry of the bodies, to understand how they are arranged in space, to evaluate the movement permitted by the joints, and to obtain a video simulation. These ports are inserted when a rigid body is added to the sketch (i.e., the schema in the software environment) and whose coordinates are added during parameterization.

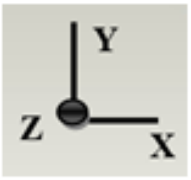
4.1.1 Inertia properties

The ports and associated parameters used to assess inertia properties are those from the CAD model. Characteristics are as follows:

• coordinate system orientation: this section presents the rotations according to the Euler decomposition (z, y, x), i.e., the first rotation around the z-axis, the second rotation around the intermediate y-axis and the third rotation around the target x-axis. In addition, these rotations can be blocked;

• position of the part considered: this window presents the coordinates of the reference system origin (designed by the letter O), the center of mass (designated by the letter G) and those of all the ports;

• inertia: values relating to the mass and the inertia matrix with respect to the body's center of mass, divided into moments of inertia around the x, y, z axes, designated as Gx, Gy and Gz respectively, representing the diagonal of the matrix, and in inertia products xy, xz, yz representing the values of the diagonal (Figure 5);



$$\begin{matrix} I_{xx} & I_{xy} & I_{xz} \\ I_{yx} & I_{yy} & I_{yz} \\ I_{zx} & I_{zy} & I_{zz} \end{matrix}$$

Figure 5 The general Simcenter Amesim inertia matrix.

• initial speeds: here, the three coordinates of initial values for absolute velocity of the center of mass and of angular velocity relative to the local orientation system can be entered. For both bodies in consideration, initial velocities were null, as the intention is to simulate movement starting from the rest position;

• advanced: in this section, the rotation mode for both rigid bodies was set to high in order to use the Euler angles and ensure faster calculation. As the axis of rotation during movement is known to be the z axis, it was chosen as the main axis of rotation. For the same reason, rotation of the center of mass along the x and y axes and its position along the z axis were limited. Numerical values for the rigid body representing the trunk with the coordinates of the two ports and the inertia values (referred to the center of gravity, trunk mass 59.43 kg) are shown together with the inertia matrix (values in kg/m^2) in Figures 13. As there are two separate subsystems connected through the hip joints, the software generates two inertia matrices, one for the upper body, and one for the lower body. The legs' mass is 35.61 kg and the inertia matrix, referred to the center of mass, is illustrated in Figures 13 (values in kg/m^2). These matrices were derived from the imported CAD geometry and automatically determined by Simcenter Simcenter Amesim after setting the correct density. At 3.29 kgm^2, the highest moment of inertia was Ixx, i.e., that along the Gx axis. This indicates that the body has greater resistance to rotation around this axis. The lowest moment of inertia was Iyy, equal to 0.53 kgm^2 in the lower body matrix. The off-diagonal moments of inertia are smaller than the diagonal moments: this indicates that mass is uniformly distributed or that the body has little tendency to rotate around two different axes simultaneously. This is also due to the movement considered here, viz., trunk flexion in the sagittal plane. It can thus be concluded that the matrix calculated by the software is consistent with the rigid body for the legs and the movements it performs.

4.1.2 The Simcenter Amesim body model

The sketch shown in Figure 6 represents the whole human body in the Simcenter Amesim environment.

From the bottom (i.e., the system ground connection), the main components are:

• zero velocity source: in Simcenter Amesim this is called zerospeedsource3D, and represents the system ground connection;

• pilot operated hinge: shown in Figure 6 with ankle joint and hip joint;

• table: this component, called dynamic time table in Simcenter Amesim, is used to interpolate data in the form of a table;

• sign inversion: in Simcenter Amesim, sign inversion reverses the sign of the data received as input;

• conversion into angular displacement and velocity signal: called null to rotary velocity and displacement units in Simcenter Amesim, this component converts a dimensionless signal into a dimensional signal;

• rotating damper spring: in Simcenter Amesim, this is called a rotary spring damper and is used to provide torque to the piloted hinges;

• zero force source: used to close the ports of the components that are not connected. As explained, analyzing model. A calls for the use of two subsystems, one for the legs and one for the upper body, from the trunk up to the head (hereinafter referred to as the trunk for convenience). The two subsystems are joined by a hinge corresponding to the hip joint, while the legs are connected to the floor through an additional point corresponding to the ankle.

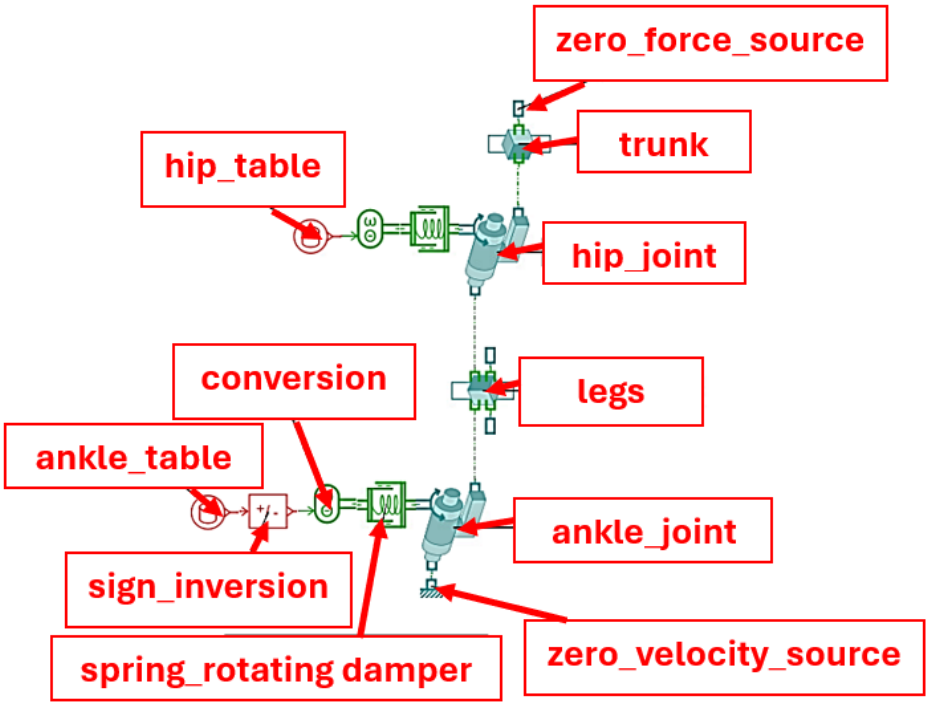
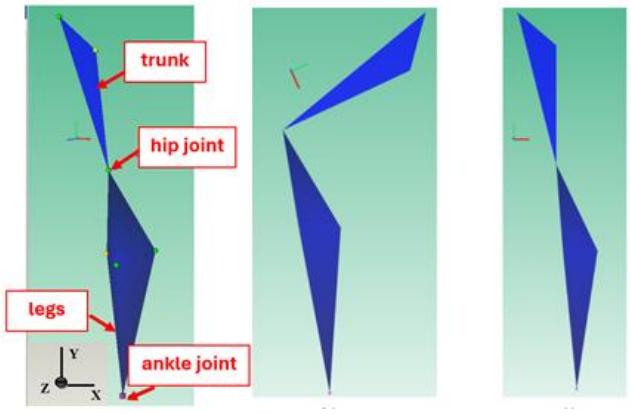


Figure 6 Sketch of the body simulated in Simcenter Amesim.

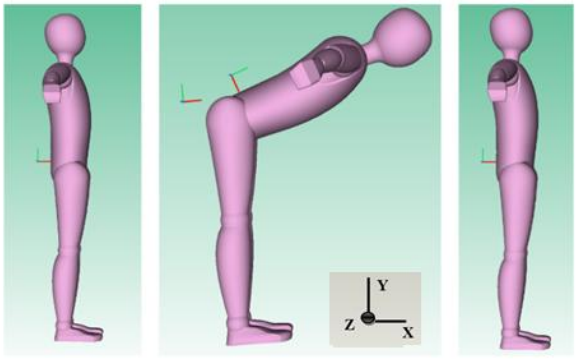
4.1.3 Trunk movement simulation

The body appears as two geometric figures, with the two rigid bodies for the legs and the trunk in blue. The geometric figures thus depend on the location of the center of mass and the location of the connecting ports (Figure 7a). Figures 7 show the video frames for the three main instants, showing how the body moves exactly as expected, i.e., with the trunk flexing forward and the legs bending backwards. The two joints that permit these movements also function correctly. The 3D body model provides a more realistic representation of body movements, as can be seen from the video frames for three different moments shown in Figure 7b.



a) b) c)

Figure 7a Trunk movement simulation in Simcenter Amesim (a) t = 0 s, b) t = 30 s, c) t = 60s) (model A).



a) b) c)

Figure 7b Trunk movement simulation with CAD human body model A (a) t = 0 s, b) t = 30 s, c) t = 60s).

In conclusion, simulations of the body model without the exoskeleton yielded the expected results, first because the body actually moves according to the setup, and also because total muscle torque at the hip is in line with the model. Torque is null when the body is upright, and reaches its maximum value when the trunk is in the position with the greatest bending angle. The hip joint was simulated using a rotary spring damper selected from the Simcenter Amesim library. In this simulation, the default values for the stiffness of the rotary spring in the ankle joint and the stiffness of the rotary spring in the hip joint were changed to 1010 Nm/degree, yielding acceptable torque values and trends for simulating muscle action. Figures 8a and 8b show trunk and leg joint angular displacements versus time. The graphs confirm that the body moves correctly in the right direction.

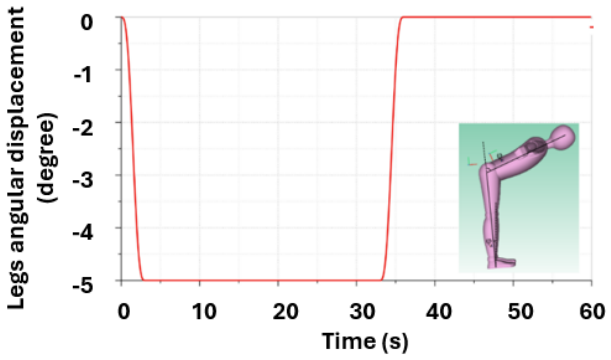


Figure 8a Leg angular displacement.

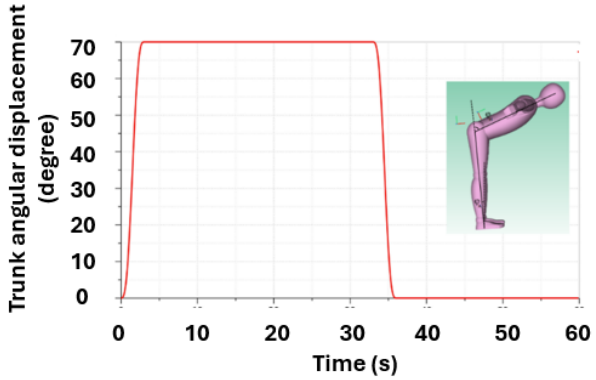


Figure 8b Trunk angular displacement.

The graphs for the trunk and the legs differ in the direction of the displacement and, consequently, the speed in order to simulate the fact that the legs bend backwards to balance body weight as the trunk bends forward. Figure 9a shows the main angles involved in these considerations. The angular displacement curves for the case where the modeled subject A is not wearing the exoskeleton are clear from Figure 9b, where it can be seen that the inflection point of the displacement occurs at x = 1.5s and y_1 = 35°, while the resulting maximum velocity at 1.5s is 7.8 rpm. These simulation results were compared with earlier theoretical and experimental results obtained by the authors on a subject without exoskeleton in the DIMEAS laboratory [12, 13] as shown in Figure 9c. Specifically, in this case the maximum bending angle of the trunk is 65° instead of 70°. The small difference between the simulation (Figure 9b) and theoretical/experimental results (Figure 9c) may be due to the different inertial properties of the human body involved. As can be seen, the two studies are in good agreement, as the angular values, behavior and time are quite similar. The graph of total muscle torque at the hip considers the z-axis torque at one of the hip ports. The hip joint was considered to be exactly centered between the two hips as shown in Figure 10, where an anatomical detail is overlaid on the body model. This location was chosen to simplify the simulation from the computational standpoint.

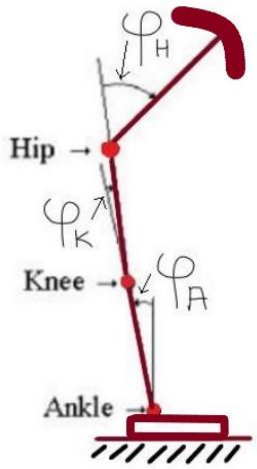


Figure 9a Details of the angles discussed in the text.

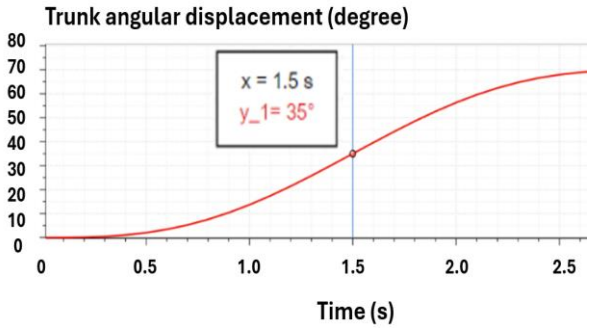


Figure 9b Trunk angular displacement obtained in Simcenter Amesim.

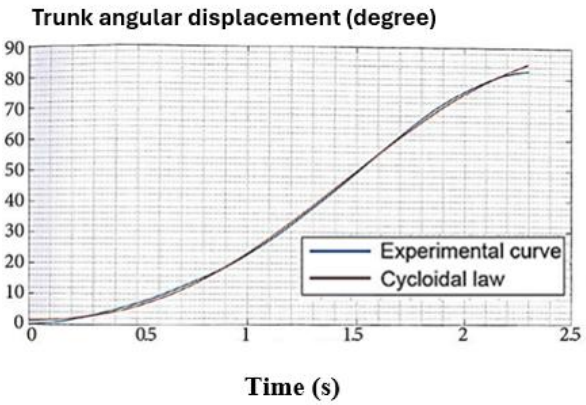


Figure 9c A previous comparison between the theoretical and the experimental cycloidal law of trunk flexion [12].

For this reason, the muscle torque at the hip is the total for both joints. This is also useful because the torque that must be input to the motor is the same for the two parts of the exoskeleton, so a single torque must also be calculated at the hip. Plotting total muscle torque at the hip was essential, as the simulation with the body model alone served specifically to visualize three-dimensional movement.

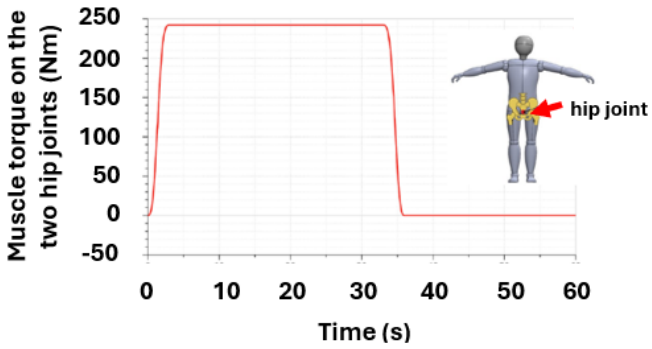


Figure 10 Simulated muscle torque on the two hip joints.

4.2 BODY MODEL B

Given the importance of the inertia matrix, the authors constructed a second human body model in a CAD environment (SolidWorks 2022) on the basis of data from the literature and ISO 7250-2 [33-35]. This model was then uploaded to Simcenter Amesim to compare its inertia matrices with those found with the first model. This second CAD human body model is shown in Figure 11a [30, 32-35], while its configuration in Simcenter Amesim is shown in Figure 11b.

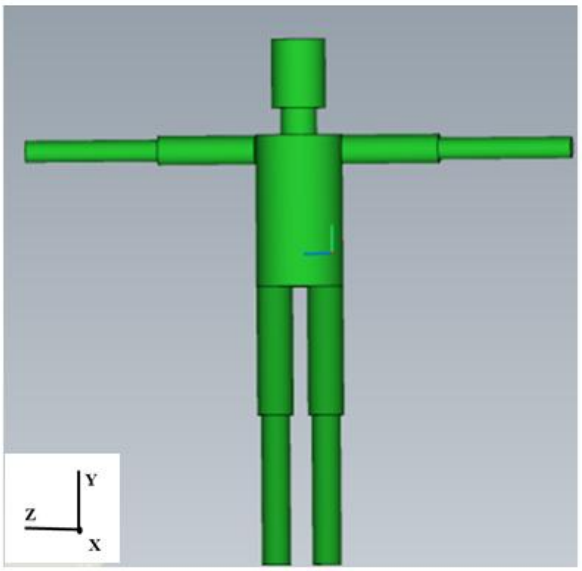


Figure 11a CAD human body model B imported into Simcenter Amesim [32, 33].

4.2.1 Inertia properties

Figure 12 shows the dynamic free body diagram of the wearer's trunk during movement. The arms are considered to be in abduction. It should be noted that the muscle torque on the hip joint is reduced by the inertial effects. During the trunk exoskeleton design process, it could thus be useful to analyze the static condition with the trunk flexed, as this makes it possible to examine a higher hip joint torque. The trunk and the leg matrices of the first and the second body models are shown in Figures 13a and 13b respectively. Values are expressed in kgm^2.

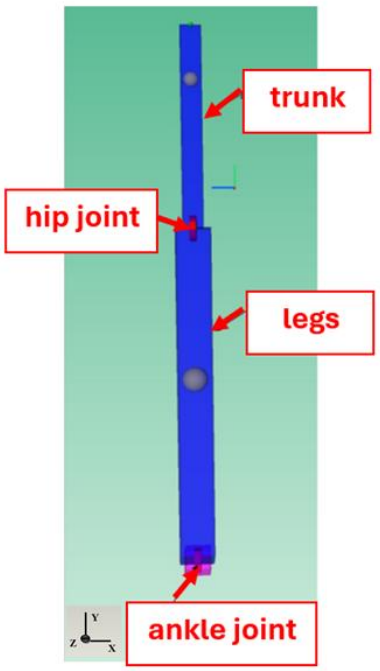


Figure 11b Human body model B in the Simcenter Amesim configuration.

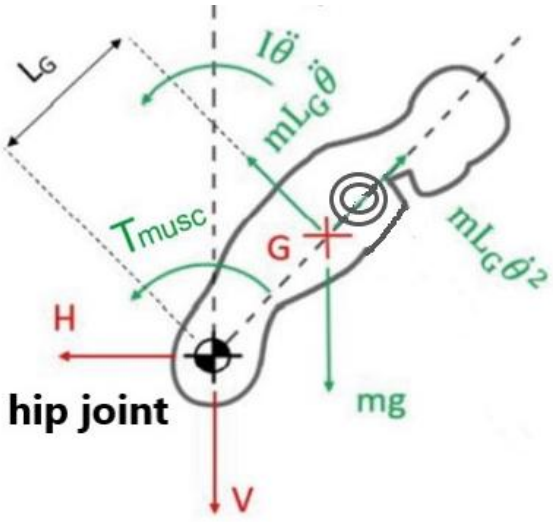


Figure 12 Dynamic free body diagram of the wearer's trunk [12].

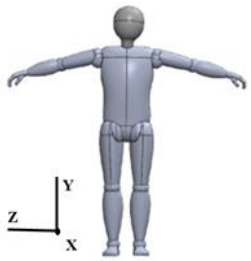
Table II shows the length of the main parts of this human body model (95%ile adult Italian male) [32-35].

Table II - Lengths of main model parts

Human part	Length (m)
Leg and foot	0.52
Thigh	0.45
Trunk	0.53
Head	0.24
Neck	0.09
Forearm	0.34
Arm and hand	0.46

The diagonal values are very similar because they are the body's main moments of inertia, which depend on the distribution of mass and shape which is very similar in the two cases.

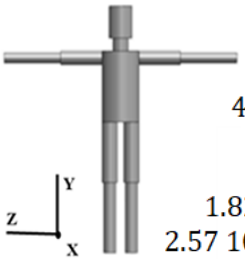
By contrast, the off-diagonal values are clearly different because they are moments of inertia of the products with respect to pairs of different axes and can vary depending on the distribution of the mass. For human body model B, products of inertia Ixy and Iyz are zero, meaning that there is no correlation between the distribution of mass along a certain axis and rotation around the other axis. This is to be expected because the mass distribution is symmetrical to the x and y axes and with respect to the y and z axes. The value of the inertia product Ixy is not exactly equal to 0, but is a very small infinitesimal (Figures 13b). In Figures 13, the diagonal values for the legs, unlike those for the trunk, differ for the two bodies. A further discrepancy between models A and B concerns the assembly. Model B features regular geometries, i.e., two cylindrical shapes respectively representing the trunk and leg subsystems, and connected by the hip joint hinge (Figure 11b). The legs' center of mass (grey dots in Figure 11b) is exactly in the center, as the legs are perfectly equal and symmetrical with no part having greater mass. For the body, the center of mass is somewhat higher because of the presence of the arms. A comparison was carried out between the model A and the model B, designed with regular shapes using the software SolidWorks 2022 and following the data provided by the standards [33-35]. The inertia matrices of this model's trunk, head, arms and legs were then compared with those for model A. The values, expressed in kgm^2, show similarities along the main diagonal of the matrices' trunk and significant differences off the diagonal. The leg matrices, however, are entirely different because of the discrepancies between the two models' volumes and masses. Moreover, unlike model A, in this case no connection ports were added at the knees because they need not be connected with the exoskeleton leg-links. To compare the total muscle torques at the hip for the two human body models, a sketch was also created for model B. As can be seen from the simulated torque curves in Figure 14, maximum torque with model B is lower than that obtained with the more realistic model, probably because of the different positions of the two models' centers of mass.



$$\begin{matrix} 5.77 & 0.14 & -0.12 \\ 0.14 & 3.29 & 0.02 \\ -0.12 & 0.02 & 2.87 \end{matrix}$$

$$\begin{matrix} 3.39 & -0.07 & -0.01 \\ -0.07 & 0.53 & 0.04 \\ -0.01 & 0.04 & 3.01 \end{matrix}$$

Figure 13a CAD human body model A and its inertia matrix in Simcenter Amesim [31].



$$\begin{matrix} 6.17 & 4.86\ 10^{-17} & 0.36 \\ 4.86\ 10^{-17} & 3.82 & 0 \\ 0.36 & 0 & 2.93 \end{matrix}$$

$$\begin{matrix} 1.82 & 2.57\ 10^{-16} & -0.02 \\ 2.57\ 10^{-16} & 0.2 & 2.77\ 10^{-17} \\ -0.02 & 2.77\ 10^{-17} & 1.66 \end{matrix}$$

Figure 13b CAD human body model B and its inertia matrix in Simcenter Amesim [32-35].

A further comparison can be based on the torque calculated from the free body diagram with the hip joint as the pole. Here the maximum total muscle torque at the hip was approximately 266 Nm [12]. This is very close to the approximately 240 Nm torque obtained with model A, and thus much lower than the theoretical value, due to the fact that the distance between the center of mass and the pole is probably different in the two cases, and also because in the theoretical case, the displacement of the center of mass during the movement was not considered to be flexion. In any case, the difference between the two maximum torques could be due to the different trunk inertia matrices for models A and B and how they interact with the muscle torque calculation, as shown in the dynamic free body diagram in Figure 12: a lower inertia effect (Figure 13a) yields a higher hip joint torque (Figure 14) referred to the model A. In the end of the paper the Table III illustrates a summary on the results and considerations obtainable about the maximum torque values.

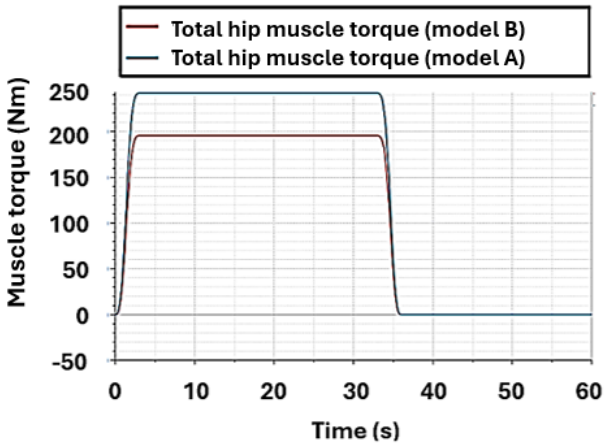


Figure 14 Some preliminary simulation results.

As inertial properties are very important for correct simulation and subsequent control system design, information for this purpose was gleaned from the literature [16, 18-29]. In [18], for example, a male subject with a height of 1.74 m, body mass of 74 kg and a trunk mass of 34.66 kg was analyzed. Mass moments of inertia were

calculated with the human body bending forward about the vertical axis with the arms extended. The trunk's moment of inertia calculated on a vertical axis passing through the chest was found to be 2.17 kgm^2, with a distance of 0.23 m between the trunk's center of mass and the shoulder joint. This value can be compared with the I_{yy} moment of inertia from the trunk matrices presented here, considering the vertical y axis and calculated during simulation (3.29 kgm^2 for body model A, 3.82 kgm^2 for model B). Taking the subjects' differing characteristics into account, the simulation result can be regarded as entirely satisfactory. In [19], a mathematical model of the human body was used to determine the mass inertial parameters of different body segments. Mass moments of inertial were calculated for a standing position with the arms hanging naturally at the sides. The model consists of 16 segments representing head + neck, upper, middle and lower torso, thigh, shank, foot, upper arm, lower arm and hand, all assumed to be relatively simple geometrical bodies. Full body symmetry with respect to the sagittal plane was assumed, and the geometrical data were taken from an anthropological investigation of the Bulgarian population [36] which measured a total of 2435 males. The average values were used to design a model representing the average Bulgarian male. For an average subject having a body mass of 98.5 kg and a height of 1.90 m, the trunk moment of inertial on the vertical axis was 1.37 kgm^2. As recent studies [16, 17] have used computer vision and techniques such as Human Mesh Recovery (HMR) in calculating the inertia properties of the upper body, the authors plan to investigate using these tools to verify the reliability of their human body models in the future. Several tasks were analyzed in the computer vision study [16]. In the first task, the person stood straight up, then flexed his elbows all the way up and then down, until returning to the neutral posture. The process was repeated three times. The second task was a shoulder rotation.
The participant stood with his upper arm abducted parallel to the ground and elbows flexed at 90° with the palms open. He then rotated his upper arm until his fingers were pointing upwards. Subsequently, the rotation was then reversed until the participant's fingers were pointing to the ground and then returned to the initial position. This task was repeated three times.

5 THE FULL MODEL

The exoskeleton model is a series of rigid bodies hinged to the two bodies representing the trunk and legs to simulate the device's interaction with the wearer's body. Input consists of the angular displacements at the hip hinge and ankles described in the previous section, plus the torque to be supplied to the motor, calculated as 30% of the total muscle torque and represented in Figure 14, where it is plotted versus time on the x-axis. This torque is transmitted to the two components that simulate the motor and divided between the two driving pulleys of the backframe and leg-link drive pulleys. For brevity only the case of the model A wearing the exoskeleton was here presented (Figure 15a). In the simulation with body model A, the stiffness of the rotary spring was 1010 Nm/degree; the stiffness of the rotary spring in the hip joint was also 1010 Nm/degree, while initial belt tension was 50 N, and belt stiffness per unit length was 17000 N/m. Tests carried out with model A wearing the simulated exoskeleton are described in detail below. The exoskeleton imported as assembled in CAD software was added to the human body model and the relative movements of all components were defined (Figure 15b). The imported CAD model features the ports described earlier, and all joined parts move together.

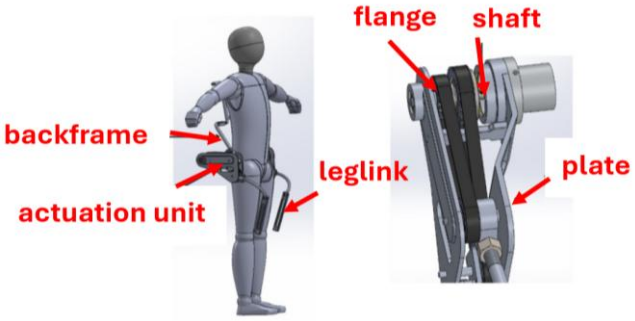


Figure 15a CAD model A and the exoskeleton with details of the actuation unit.

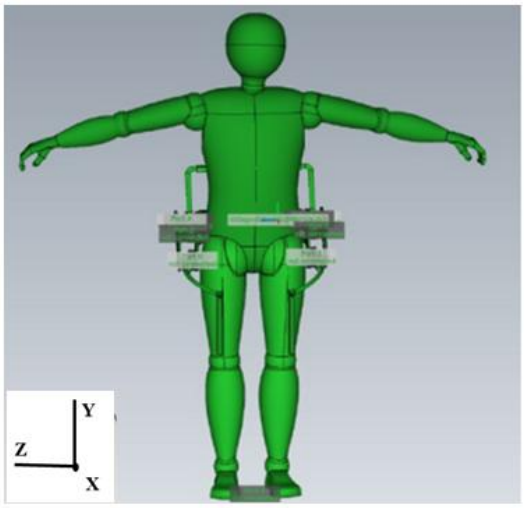


Figure 15b CAD model A with the exoskeleton (Simcenter Amesim environment).

Figure 16 shows the sketch of the operator wearing the exoskeleton. The actuation units were simulated by means of a sketch with the left and right actuation unit models. The exoskeleton model (Figure 16) consists of right/left flange, backframe drive pulley, backframe, reducer, counterplate, right/left shaft, right/left leg-link pulley, right/left plate, right/left leg-link, and right/left leg-link pulley. The two actuation units were connected by means of the wearer's trunk, the backframe, the legs, and the ankle joint. Each motor received 30% of the maximum hip muscle torque. Motor torque was reduced from maximum

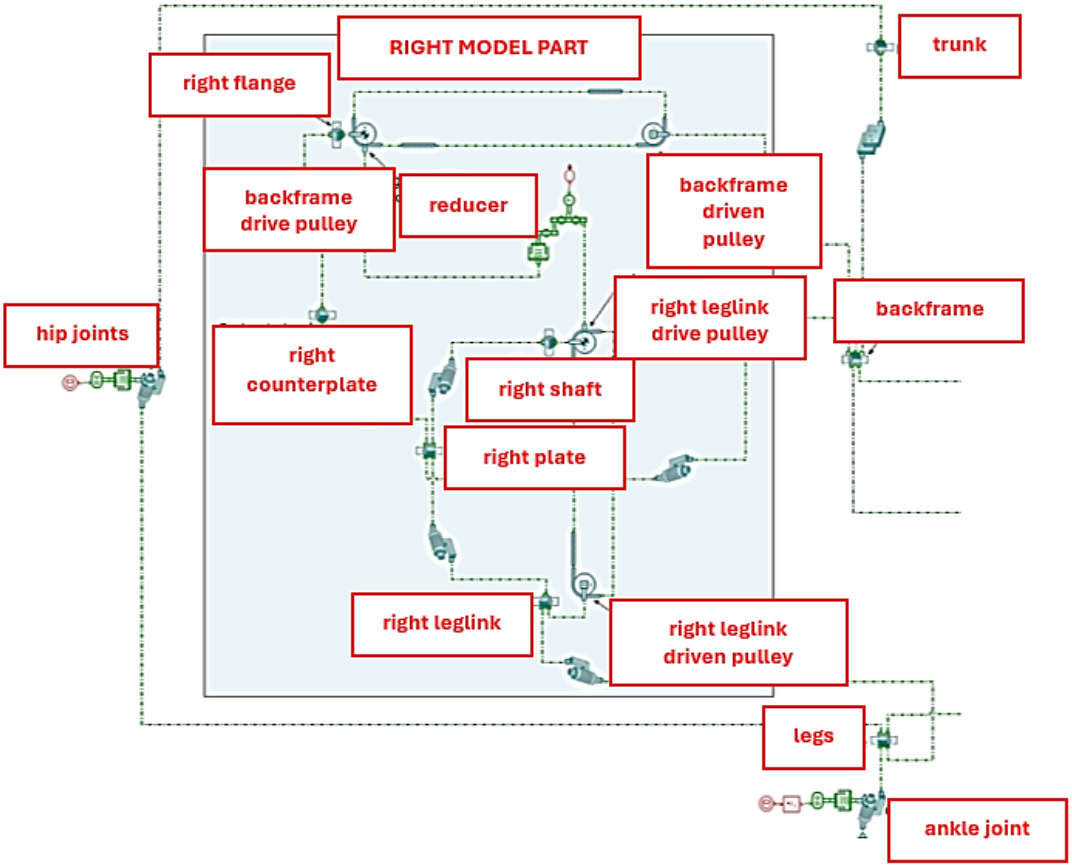


Figure 16 Simcenter Amesim sketch of the wearer and exoskeleton.

by a gain block, and delivered by a transmitter block. The main components simulating the motor include the reducer and a rotary spring providing torque to the backframe and leg-link drive pulley. The blocks representing the belt drives were then created. In these blocks, the drive pulleys have their own inertia parameters with a structure providing motor torque on the inlet port and the pulley velocity on the outlet port. The driven pulleys' angular velocity is delivered by the port connected to the backframe and the leg-link. As mentioned above, the main purpose of this simulation is to check that the total muscle torque at the hip is 70% of that calculated with the human body model alone, given that the exoskeleton serves to reduce muscle fatigue.

6 PRELIMINARY SIMULATION RESULTS

The assembled bodies can now be visualized to understand how they move relative to each other and whether the simulation leads to correct flexion as provided in input. The rigid bodies are seen as different geometric figures based on the location of the center of mass and ports (Figures 17 a, b, c). Total muscle torque at the hip, in this case, is influenced by the stiffnesses provided to the rotary spring component as well as by the drive belts' initial tension and stiffness. For example, increasing initial belt tension increases the maximum torque, which would thus exceed what it should be for the exoskeleton to actually reduce the wearer's muscle fatigue. An average value of the maximum torque on each hip joint in the case of the wearer (model A) with full exoskeleton is about 88 Nm. It is interesting to see what angles are assumed by the exoskeleton components as they move together with the wearer's body.

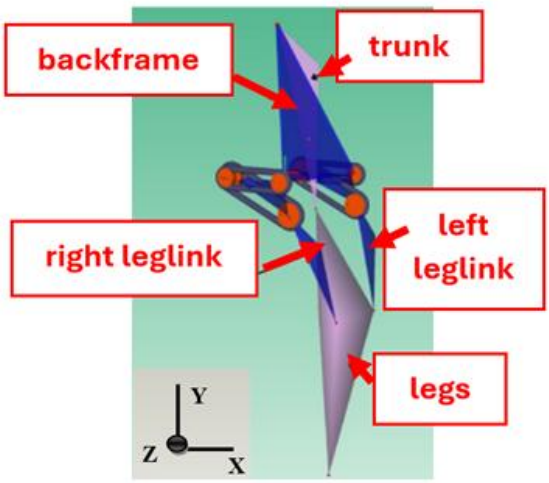


Figure 17a Simcenter Amesim model A of the wearer with exoskeleton and actuation units (side view).

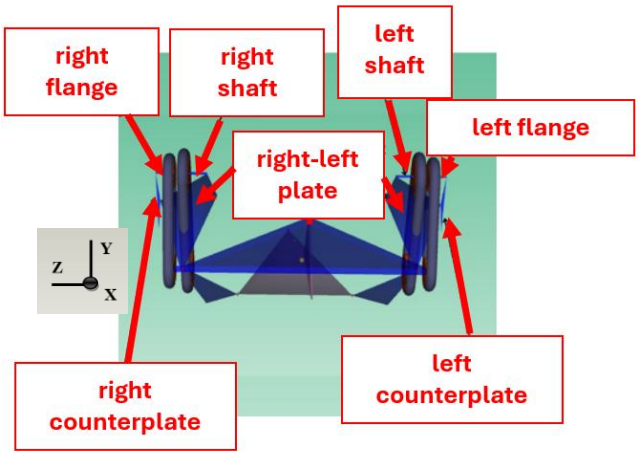


Figure 17b Simcenter Amesim model A of the wearer with exoskeleton and actuation units (top view).

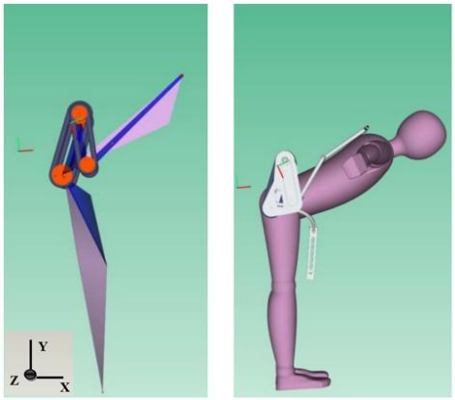


Figure 17c Simcenter Amesim model A of the wearer with full exoskeleton. Right: CAD representation.

Figure 18a shows leg-link angular displacement, while Figure 18b shows backframe angular displacement. The latter in particular is in good agreement with previous experimental studies [11, 12]. The negative sign is due to the clockwise rotation imposed to the motor. The backframe angular displacement curve takes into account instants with non-constant velocity, and thus with accelerations as shown in the dynamic free body diagram in Figure 12.

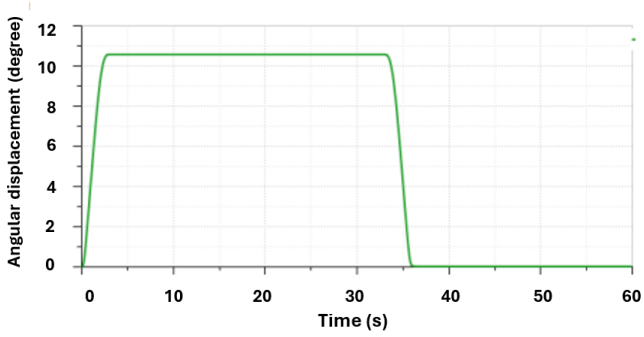


Figure 18a Leg-link angular displacement.

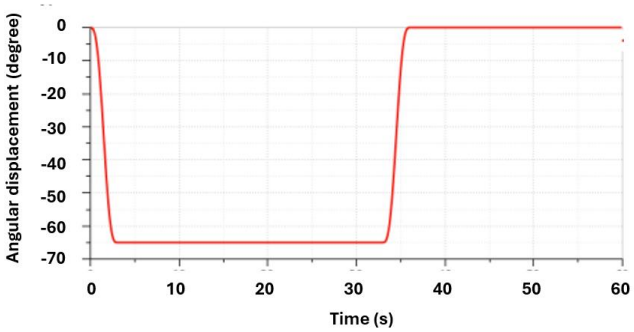


Figure 18b Backframe angular displacement.

7 COMPARISON WITH PREVIOUS MODELS BY THE AUTHORS

In earlier work, the authors modeled a human trunk wearing this exoskeleton using Matlab (2020 version) and Simulink (2020 version) software [12, 13]. This model was based on the trunk dynamic free body diagram (Figure 12) and its dynamic equilibrium. Figure 19a shows this model. The model consists of the wearer's trunk, the control system for each pneumatic motor with its proportional solenoid valve, and an angular position input for speed and acceleration. The control system must ensure correct exoskeleton function as the wearer's trunk bends forward, is held in the forward position, and returns upright. The control system is designed so that the motor delivers 30% of maximum muscle torque. Position and temperature sensors are also provided. The red circle indicates the pneumatic motor, whose extended model is illustrated in Figure 19b. In general, this control system must guarantee that the angular position, angular velocity and angular acceleration sensors are read correctly together with the physiological torque in play at all times, and that the motors for each hip joint are appropriately controlled. In addition, control logic must be simple and parts must be lightweight so as not to burden the wearer. Control logic covers the four stages of exoskeleton operation, which include a stage controlled by a position sensor in which the mechanism is locked to support the trunk while the wearer bends forward in a stationary position. If the operator's trunk flexes less than 20°, trunk movement is considered along with that of the pelvis, while for flexion exceeding 20° the pelvis is considered rotated 20° from its position when the operator is standing and the trunk continues to bend forward up to a maximum of 70° from the vertical. In this stage, a speed sensor senses when the wearer's trunk is bent forward and stationary, and activates the actuation group to generate the torque needed to support it. When the speed sensor senses that the wearer's trunk begins to return to the upright position, the control system acts to assist this movement. The model used in an earlier study to investigate the trunk flexion system is illustrated in Figure 19b, which shows the reducer i_rid, the motor characteristic, the correction factor, and torque feedback T_{FB}.

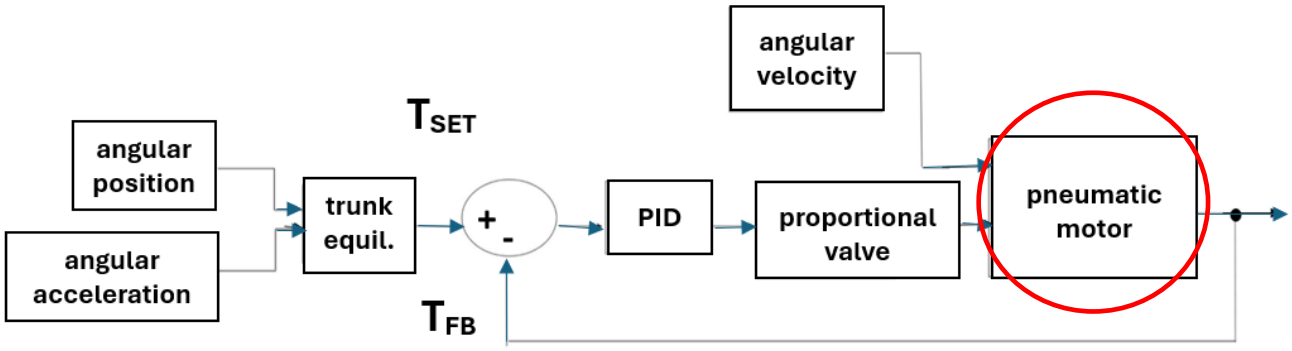


Figure 19a The authors' previous model of the entire "wearer + exoskeleton + pneumatic motor control" system [13].

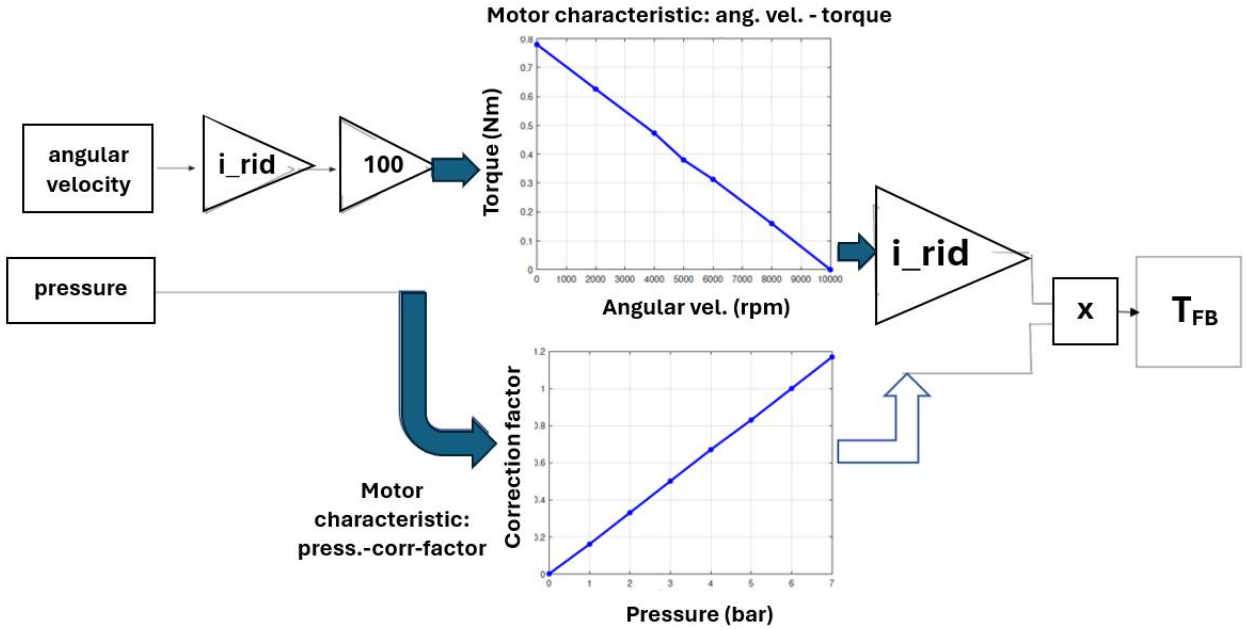


Figure 19b The authors' previous model of the exoskeleton actuation unit (pneumatic motor) [13].

As shown in the figure, this model controls the actuation unit using two graphs (supplied by the motor manufacturer) of motor torque versus angular velocity and of the motor correction factor versus pressure. The "i_rid" block shown before and after these characteristic curves simulates the harmonic drive used in each actuation unit, which reduces the angular velocity but increases torque by a factor of 100. Each pneumatic motor, which generates 30% of the maximum muscle torque to support the wearer's trunk, is controlled via an electro-pneumatic proportional valve.

As explained in [12,13] the pneumatic control circuit can be essentially made of a pneumatic source, a filter, a proportional valves, the air motor. The discharged of the air motor can be stopped during the operator's trunk flexion stable phase, in order to sustain it for all the time required. Figure 19c shows a possible layout of this pneumatic control system, where: (1) is the pneumatic source; (2) is the filter; (3) is a control direction flow valve 4/2; (4) is a manometer; (5) is a proportional valve; (6) is the air motor. In this scheme the components (3) and (4) are only useful for experimental tests carried out in laboratory. In it there are: source (1); a filter (2); a control direction flow valve 4/2 (3); a manometer (4); a proportional valves (5); the air motor (6).

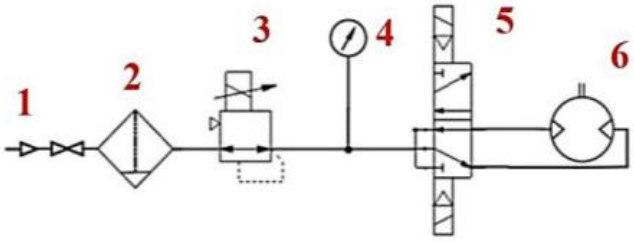


Figure 19c A possible layout of the pneumatic control system [12,13].

The choice of a pneumatic actuation has been made for the advantages it offers, such as: high power-to-weight ratio, possibility to work in dirty and explosive atmospheres, greater comfort and safety, linked to the compressibility of the air. The pressure output of the proportional valve is obtained by varying its input voltage from 0 to 10 V, producing a maximum pressure of 6 bar (1 bar = 10^5 Pa) to power the pneumatic motor. Each pneumatic motor is driven by a PID controller, where proportional (k_P) and integrative gains (k_I) equal to k_P = 0.8 and k_I = 5 ensure system stability and accuracy. Figures 20 show the torque on the total hip joints obtained in the various simulations.
Figure 20a shows the torque obtained through the simulation. The figure compares the feedback torque signal from the air motor (T_{FB}) and the set muscle torque (T_{SET}). The two curves are very similar, with practically negligible error. This error has two peaks as the wearer's trunk flexes forward and returns upright. In any case, error is minimal and causes no disturbance in system operation. In particular, proportional valve control voltage rises to a maximum when the trunk is at maximum flexion, when maximum torque is required. The supply pressure of each air motor also increases along with proportional valve control voltage. The torque designated as T_{SET} in Figure 20b was the torque on the hip joint obtained from the dynamic trunk equilibrium and equal to the 30% of maximum muscle torque. Its behavior and maximum value is in good agreement with the corresponding torque in Figure 20c, demonstrating that the two models using different structures and software packages function correctly. The few differences between maximum torques may be due to the inertia parameters used in the models, which were taken directly from the Simcenter Amesim inertia matrices in some cases, and from the trunk free body diagram and from the trunk dynamic equilibrium in others. As the hip joint torque value and curve demonstrate, the new models presented here and earlier ones are comparable. This is encouraging, both as a preliminary validation of the new model and in terms of being able to use two different but equally valid models.

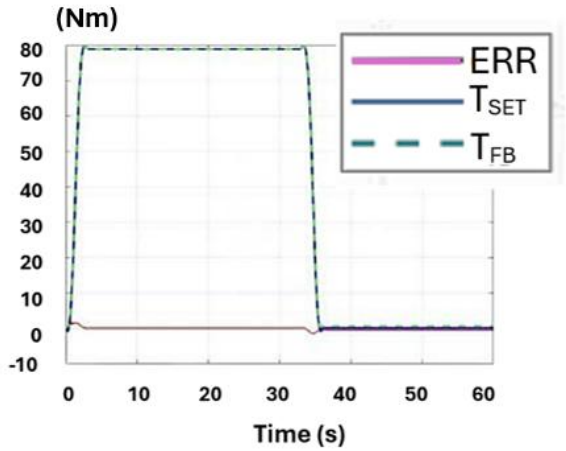


Figure 20a Torque curve and error obtained from the previous model [13].

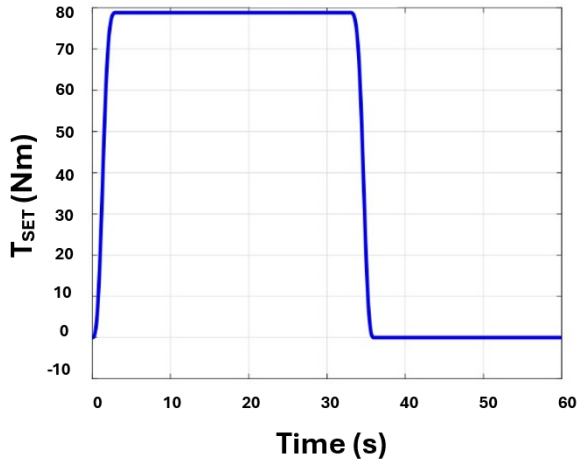


Figure 20b Motor torque curve from the previous model[13].

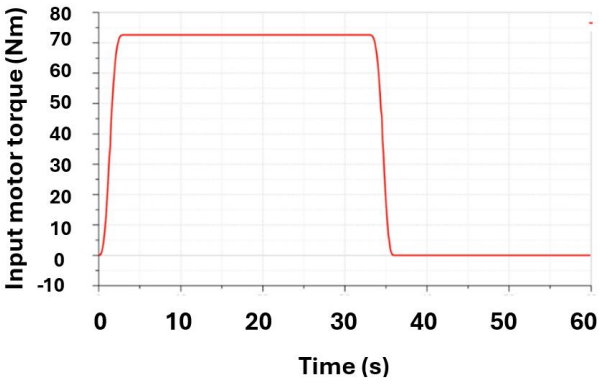


Figure 20c Motor torque curve from the Simcenter Amesim wearer and exoskeleton model.

Table III - A summary on the maximum torques values obtained on each hip joint

Maximum torque	Numerical value (Nm)
Operator without exoskeleton (human model A, Simcenter Amesim enviroment)	123
Operator without exoskeleton (human model B, Simcenter Amesim enviroment)	98
Wearer (model A) with full exoskeleton (Simcenter Amesim environment)	72
Wearer (equilibrium from free body diagram) with full exoskeleton (Matlab and Simulink 2020 environment)	79

Table III illustrates a useful comparison among the various maximum torques values obtained in the presented studies.The differences among the various maximum torque values could be attributed to the different inertial matrices constructed in Simcenter Amesim referring to the two human models (A and B) proposed in the literature [32] without exoskeleton. The addition of this one increased the

inertia torque in this phase of trunk flexion and acceleration downwards, reducing the torque required on each hip joint. A similar situation arises in the case of a model in Matlab-Simulink 2020 environment. This can precisely confirm the inertial effect linked to the presence of the exoskeleton.

8 CONCLUSIONS

The evaluation of inertias is a fundamental aspect in the design of exoskeletons and their control systems. In this paper the author aims to present a particular study on the inertias of the upper body, using various CAD models, made according to literature and examining the inertial aspects both in the case of the body alone and in the case of the operator wearing an exoskeleton. So the simulation presented here made it possible to evaluate the behavior of an exoskeleton in interaction with the human body during flexion and extension, and when standing while bent forward. The results verified that the exoskeleton performs its intended purpose by evaluating the total muscle torque at the hip, which was 30% less than that obtained during body flexion and extension without the device. The results obtained were appropriately compared with similar studies present in the literature and the comparison always gave satisfactory results. A comparison with earlier numerical models of the "wearer + exoskeleton" system yielded good results and shows that all the models are reliable. This also provides various types of models and simulation possibilities with different software also useful for future studies with other types of exoskeletons. The study carried out by the author can produce an interesting method of study on this argument. Such models and analyses can also be useful for ergonomic considerations. Future work will focus on optimizing the motor model, for example by using the Simcenter Amesim pneumatic library, designing the control system, optimizing the drive system through detailed studies of the friction coefficients between the belt and pulley, elongations and tensions, and on using new AI-based tools such as computer vision and Human Mesh Recovery for experimental inertia analysis. Currently, many studies on the topic are conducted with various AI software, also based on the human body pose estimation. Other work currently centers on calculating mass moments of inertia for comparison with those presented here in order to improve Simcenter Amesim simulations. In the future it may be possible to evaluate the possibility of setting up models that are also useful for understanding the actual interaction between the human body and the exoskeleton and the stresses that it produces on the body itself. Further studies are underway by the authors to deepen the calculation of the inertia matrix in SimCenter Amesim, analyzing various positions of the human body and comparing the results obtained with appropriate literature papers where similar subjects and positions are examined.

ACKNOWLEDGEMENTS

The author would like to thank Prof. Terenziano Raparelli, BSIM Italy (Turin, Italy) and Eng. M. Ancona for their help during this study.

REFERENCES

[1] Pons J.L., *Wearable robots: biomechatronic exoskeletons*. Vol. 70. Wiley Online Library, 2008.

[2] Belforte G., Eula G., Appendino S. and Sirolli S., Pneumatic Interactive Gait Rehabilitation Orthosis: design and preliminary testing. *Proc. of the Institution of Mechanical Engineers, Part H: Journal of Engineering in Medicine*, Vol. 225, No. 2, pp. 158-169, 2011.

[3] Harman E. A. and Frykman P. N., Heavy load carriage performance correlates: backpack vs individual towed trailer. *Medicine & Science in Sports & Exercise*, Vol. 27, No. 5, S136, 1995.

[4] Christensen S., Rafique S. and Bai S., Design of a powered full-body exoskeleton for physical assistance of elderly people. *International Journal of Advanced Robotic Systems*, Vol. 18, No. 6, pp. 1-15, 2021.

[5] Belforte G., Eula G., Sirolli S., Appendino S., Geda E., Geminiani G., Zettin M., Virgilio R. and Sacco K., Control curves for a new lower limbs robotic exoskeleton obtained from the study of joints angles during an unloaded human walking. *International Journal of Mechanics and Control (JoMac)*, Vol. 18, No. 01, pp. 3-14, 2017.

[6] Belforte G., Raparelli T., Eula G., Sirolli S., Appendino S., Geminiani G.C., Geda E., Zettin M., Virgilio R. and Sacco K., Study and realisation of a preliminary control system for the active exoskeleton called P.I.G.R.O., suitable for unloaded robotic neurorehabilitation treatments. *International Journal of Mechanics and Control (JoMac)*, Vol. 22, No. 01, pp. 125-142, 2021.

[7] Belforte G. and Eula G., Design of an active-passive device for human ankle movement during functional magnetic resonance imaging analysis. *Proc. of the Institution of Mechanical Engineers, Part H: Journal of Engineering in Medicine*, Vol. 226, No. 1, pp. 21-32, 2011.

[8] Wu Q., Wang X., Du F. and Zhang X., Design and control of a powered hip exoskeleton for walking assistance. *Int. Journal of Advanced Robotic Systems*, Vol. 12, No. 18, p. 1-12, 2015.

[9] Hara H. and Sankai Y., Development of HAL for lumbar support. *SCIS & ISIS 2010 - Joint 5th Int. Conf. on Soft Computing and Intelligent Systems and 11th International Symposium on Advanced Intelligent Systems*, December 8-12th Okayama Convention Center, Okayama Japan, pp. 416–421, 2010.

[10] Abane A., Guiatni M., Ababou N., Amine Alouane M. and Bouzid Y., Mechatronics Design and Control of a Transformed Upper Limb Rehabilitation Exoskeleton. *International Journal of Mechanics and Control (JoMac)*, Vol. 21, No. 01, pp. 75-90, 2020.

[11] Raparelli T., Eula G., Mazza L., Ivanov A., Pietrafesa F., Mala R. and Pontin M., A preliminary prototype of an industrial exoskeleton for the operator's trunk support. *International Journal of Mechanics and Control* (*JoMac)*, Vol. 23, No. 02, pp. 37-52, 2022.

[12] Raparelli T., Eula G., Mazza L., Ivanov A., Pietrafesa F., Mala R. and Pontin M., The design of an innovative active exoskeleton prototype for industrial application with a pneumatic actuation. *International Journal of Mechanics and Control*, Vol. 23, No. 02, pp. 61-72, 2022.

[13] Raparelli T., Mazza L., Eula G. and Pietrafesa F., Sistema di controllo per un esoscheletro industriale ad azionamento pneumatico. *Oleodinamica Pneumatica, ed. Tecniche Nuove Italia*, December 2022, pp. 24-29, 2022.

[14] Raparelli T., Mazza L. and Eula G., Study concerning design and optimization of a multifunction actuation group for an industrial exoskeleton. *IFIT 2024 Politecnico di Torino (IFToMM Italy 2024)*, Turin, Italy, Vol. II, Chapter 1, MMS 164, 2024.

[15] Huysamen K., Power V. and O'Sullivan L., Elongation of the surface of the spine during lifting and lowering, and implications for the design of an upper body industrial exoskeleton. *Applied Ergonomics*, Vol. 72, No. 4, pp. 10-16, 2018.

[16] Menychtas D., Glushkova A. and Manitsaris S., Extracting the Inertia Properties of the Human Upper Body Using Computer Vision. *Computer Vision Systems* 12th International Conference, ICVS 2019, Thessaloniki Greece, September 23–25, Vol. 11754, pp. 596-603, 2019.

[17] Muhammad Z.U.D., Huang Z. and Khan R., A review of 3D human body pose estimation and mesh recovery. *Digital Signal Processing*, Vol. 128, No C, pp. 1-22, 2022.

[18] Krishnan R.H., Devnandh V., Brahma A.K. and Pugazhenthi S., Estimation of mass moment of inertia of human body, when bending forward, for the design of self-transfer robotic facility. *J. of Eng. Science and Technology*, Vol. 11, No. 2, pp. 166-176, 2016.

[19] Nikolova G. Kotev V. and Dantchev D., CAD design of human male body for mass-inertial characteristics studies. *NCTAM 2017, MATEC Web of Conferences*, Vol. 145, 04006, pp. 1-6, 2018.

[20] Drillis R., Contini R. and Bluestein M, Body segment parameters: a survey of measurement techniques. *Digital Resource Foundation O&P Library Artificial Limbs*, Vol. 8, No. 1, pp. 44-66, 1964.

[21] Bova M., Massaro M. and Petrone N., A three-dimensional parametric biomechanical rider model for multibody applications. *Applied Sciences MDPI*, Vol. 10, No. 13, pp. 1-25, 2020.

[22] Bogovic S., Stjepanovic Z., Cupar A., Jevsnik B., Regina-Car B. and Rudolf A., The use of new technologies for the development of protective clothing: comparative analysis of body dimensions of static and dynamic postures and its application. AUTEX Research Journal, Vol. 19, No. 4, pp. 301-311, 2019.

[23] Fan Y., Li Z. and Lv C., Calculation of mass and inertia moment of human body in motion by means of transformation matrix. *Proc. of SPIE, The International Society for Optical Eng*., Vol. 7128, pp. 1-8, 2008.

[24] Liu L., Cooper J.L. and Ballard D.H., Computational modeling: human dynamic model. *Frontiers in Neurorobotics,* Vol. 15, pp. 1-36, 2021

[25] Ma Y., Kwon J., Mao Z., Lee K., Li Linlin and Chung H., Segment inertial parameters of Korean adults estimated from three-dimensional body laser scan data. *Int. J. of Industrial Ergonomics*, Vol. 41, No. 1, pp. 19-29, 2011.

[26] Dodig M., Models and modelling of dynamic moments of inertia of human body. *International Journal of Sprots Science*, Vol. 6, No. 6, pp. 249-256, 2016.

[27] Paletta L., Santner K, Fritz G., Hofmann A., Londron G., Thallinger G. and Mayer H., FACTS—A computer vision system for 3D recovery and semantic mapping of human factors. *In: Chen, M., Leibe, B., Neumann, B. (eds) Computer Vision Systems. ICVS 2013. Lecture Notes in Computer Science ed. Springer, Berlin, Heidelberg*, Vol. 7963, pp. 62-72, 2013.

[28] Liang W., Inertia parameters of human body identification by using the inequality constraints derived from the dynamic equations. *Proceedings of the 2018 IEEE, Int. Conf. on Cyborg and Bionic Systems (CBS)*, Shenzhen China, 25-27 October, pp. 549-553, 2018.

[29] Robert. T., Leborgne P., Abid M., Bonnet V., Venture G. and Dumas R., Whole body segment inertia parameters estimation from movement and ground reaction forces: a feasibility study. *Computer Methods in Biomechanics and Biomedical Eng.*, Vol. 20, No. s1, pp. 175-176, 2017.

[30] https://bsim-engineering.com/

[31] https://grabcad.com/

[32] Herman I.P., *Physics of the Human Body.* Springer 2nd Edition, pp. 1-980, 2016.

[33] ISO 7250-1:2017 (Main) Basic human body measurements for technological design—Part 1: Body measurement definitions and landmarks, 2017.

[34] UNI EN ISO 7250-1:2010. Basic human body measurements for technological design—Part 1: Body measurement definitions and landmarks, 2010.

[35] UNI EN ISO/TR 7250-2:2010. Basic human body measurements for technological design—Part 2: Statistical summaries of body measurements from individual ISO populations, 2010.

[36] Izdatelstvo A., *Anthropology of the Bulgarian population at the end of the 20th century (30-40 years old persons).* ed. Yordanov Yordan, pp. 1-431, 2006.